

JGR Space Physics

RESEARCH ARTICLE

10.1029/2020JA028971

Key Points:

- Juno-UVS discovered expanding auroral emission circles with typical brightness up to 140 kR
- The features are located in the auroral swirl region, magnetically mapping to the outer magnetosphere
- Their origin would be consistent with dayside reconnection or signatures of Kelvin-Helmholtz instabilities

Supporting Information:

- Supporting Information S1
- Movie S1
- Movie S2
- Movie S3
- Movie S4

Correspondence to:

















V. Hue,
vhue@swri.org

Citation:

Hue, V., Greathouse, T. K., Gladstone, G. R., Bonfond, B., Gérard, J.-C., Vogt, M. F., et al. (2021). Detection and characterization of circular expanding UV-emissions observed in Jupiter's polar auroral regions. *Journal of Geophysical Research: Space Physics*, 126, e2020JA028971. <https://doi.org/10.1029/2020JA028971>

Received 25 NOV 2020
 Accepted 27 FEB 2021

Detection and Characterization of Circular Expanding UV-Emissions Observed in Jupiter's Polar Auroral Regions

V. Hue¹ , T. K. Greathouse¹ , G. R. Gladstone^{1,2} , B. Bonfond³ , J.-C. Gérard³ , M. F. Vogt⁴ , D. C. Grodent³ , M. H. Versteeg¹ , J. A. Kammer¹ , G. Clark⁵ , R. W. Ebert^{1,2} , R. S. Giles¹ , M. W. Davis¹ , K. Haewsantati^{3,6,7} , S. J. Bolton¹ , S. M. Levin⁸ , and J. E. P. Connerney^{9,10} 

¹Southwest Research Institute, San Antonio, TX, USA, ²University of Texas at San Antonio, San Antonio, TX, USA, ³STAR Institute, LPAP, Université de Liège, Liège, Belgium, ⁴Center for Space Physics, Boston University, Boston, MA, USA, ⁵Johns Hopkins University Applied Physics Laboratory, Laurel, MD, USA, ⁶Ph.D. Program in Physics, Department of Physics and Materials Science, Faculty of Science, Chiang Mai University, Chiang Mai, Thailand, ⁷National Astronomical Research Institute of Thailand (Public Organization), Chiang Mai, Thailand, ⁸Jet Propulsion Laboratory, Pasadena, CA, USA, ⁹Space Research Corporation, Annapolis, MD, USA, ¹⁰NASA Goddard Spaceflight Center, Greenbelt, MD, USA

Abstract Jupiter's polar auroral region hosts UV auroral emissions that relate to the magnetospheric dynamics from the outer magnetosphere. Juno-UVS has discovered intriguing features characterized by expanding emission circles of UV-brightness <140 kR. These events are located at the border of the previously defined swirl region, nearby the polar dark region. The features expand into a circular shape up to ~1,000 km in radius, at expansion velocities from 3.3 ± 1.7 up to 7.7 ± 3.5 km/s, as measured over the four best observed cases. Using color ratio measurements as a proxy for the depth of the recorded features, the mean electron energy responsible for these emissions is 80–160 keV. Events occurring in the outer magnetosphere at distances >100 R_J are likely causing for these features. Dayside magnetopause reconnection and Kelvin-Helmholtz instabilities resulting from the shear flows near the magnetopause are expected to generate field-aligned currents that could potentially be the cause of these features.

1. Introduction

The magnetosphere-ionosphere coupling at Jupiter produces the brightest UV aurora in the solar system. These emissions result from precipitating charged particles at high latitudes. Extensive monitoring of these emissions using Earth-orbiting observatories, as well as flyby and orbiting spacecrafts, revealed that they can be used as a remote proxy for various magnetospheric processes. The different components of the auroral emissions reflect the various processes occurring throughout the magnetosphere. They range from the lower latitude auroral emissions caused by the satellite-magnetodisk interactions, to the high-latitude polar auroral emissions, related to the outer magnetosphere dynamics as well as the interaction region with the solar wind (e.g., Badman et al., 2015; Clarke et al., 2004; Grodent, 2015).

Prior to Juno, Jupiter's polar UV emissions as viewed from an Earth-orbiting perspective have mainly been classified into three sub-regions: the active, the dark and swirl regions. The dark region generally appears dark in the UV, and is characterized by a crescent of faint H₂ emission (<10 kR; e.g., Grodent, 2015; Nichols et al., 2009a). It is located between the main auroral ovals and the center of the polar aurora on the dawn side, and is known to significantly vary in size and location, sometimes extending toward the dusk side (Nichols et al., 2007; Swithenbank-Harris et al., 2019). It is thought to be linked to the sunward return flow of depleted flux tubes emptied out by Vasyliūnas-reconnection as they rotate toward the nightside magnetosphere (Kivelson & Southwood, 2005; Vasyliūnas, 1983). The active region is characterized by highly dynamic bright flares and arc-like structures (e.g., Nichols et al., 2007; Nichols et al., 2017a). It is thought to be linked to the polar cusp or possibly driven by an increase in the solar-wind ram pressure (e.g., Grodent, 2015). Grodent et al. (2003) interpreted the bright polar flares as driven by dayside magnetopause reconnection, while the arc-like structure may possibly be the signature of the Dungey-cycle X-line (Cowley et al., 2003; Dungey, 1961). These interpretations were later challenged by the finding of conjugacy in the

active region, indicating that these regions corresponded to closed field lines (Bonfond et al., 2016). Finally, the swirl region encompasses the area of bright patchy auroral emission characterized by swirling motion, roughly located at the center of the polar auroral region, and sometimes showing the presence of quasi sun-aligned polar auroral filaments (Nichols et al., 2009b). It is thought to be a region of open magnetic field lines (e.g., Grodent, 2015).

Observations of Jupiter's auroral emission with the Hubble Space Telescope (HST) have allowed numerous transient features to be highlighted. Patches of UV emission with typical spatial extent of $\sim 1,000$ km and X-ray auroral pulses were found poleward of the main emission (Branduardi-Raymont et al., 2008; Pallier & Prangé, 2001). They are thought to trace the region of open magnetic flux and are possibly triggered by dayside reconnection (Bunce et al., 2004). Grodent et al. (2003) identified an auroral flare located inside the active region, and suggested that such flares could be related to burst-like reconnection processes associated with a flux transfer event that allows momentum exchange from the solar wind to the magnetosphere. Quasi-periodic (2–3 min) flares in the southern polar auroral region were located on the dusk side of the main emission inside the active region (Bonfond et al., 2011). Using the magnetic flux mapping of Vogt et al. (2011), Bonfond et al. (2011) showed that these flares map to the outer magnetosphere, at equatorial distances of 55–120 Jovian radii (R_J), and to local times from 10:00 to 18:00. By analogy with similar features detected in the Earth's magnetosphere, they suggested these flares originate from pulsed-dayside reconnections. During an additional HST campaign, quasi-periodic flares in the active region were observed to occur in phase between the two hemispheres (Bonfond et al., 2016). This conjugacy led Bonfond et al. to suggest that these emissions took place on closed field lines instead.

Infrared (IR) H_3^+ emission of the polar aurora provides a complementary view to understand the magnetospheric physics at work. The distinct auroral regions observed in the IR were summarized by Delamere et al. (2015). Overlapping with the UV swirl region is the fixed dark polar region (f-DPR), a region of stagnant ionospheric flow, found to co-rotate with the magnetic pole (Stallard et al., 2003), whose origin is still debated. While Cowley et al. (2003) and Stallard et al. (2003) identified this region as mapping to open field lines, Delamere and Bagenal (2010) suggested instead that the f-DPR is connected with tailward flows in the interaction and cushion regions, that is, the region containing both solar wind and magnetospheric ions, and the region of depleted flux tubes following a Vasyliūnas cycle, respectively. It is worth noting here that recent ground-based observations may suggest that the location of the f-DPR could change over time, as it was more recently found to be collocated with the UV dark region (Johnson et al., 2017). The UV dark region corresponds to the IR rotating dark polar region (r-DPR), a region of subrotational ionospheric flows (Stallard et al., 2003). That region is interpreted as the sunward return flow of depleted flux tubes following a Vasyliūnas cycle (Cowley et al., 2003), though its origin is also debated (Delamere & Bagenal, 2010).

The perspective of the Jovian auroras offered by HST provides a biased view of the auroral morphology, as it is restricted to dayside observations. The Juno mission, in orbit around Jupiter since July 2016, has provided an entirely new perspective on the morphological study of the Jovian auroras (Connerney et al., 2017) using Juno-UVS (UVS hereafter), a photon-counting imaging spectrograph (Gladstone et al., 2017a). For instance, UVS provided unprecedented views from above both poles at local times unachievable from HST (Bonfond et al., 2017). It also provided a monitoring of the total auroral power as Juno entered the Jovian magnetosphere (Gladstone et al., 2017b).

Perijove after Perijove (PJ hereafter), UVS has revealed drastically different auroral morphologies both in the north and the south. One of the most striking discoveries so far is the local-time dependence of the polar auroral intensities and spectral characteristics. Observations of the polar aurora over a wide range of local times showed a strong dichotomy of the northern polar auroral emissions at noon versus at midnight, as the emissions appear to turn off between local time from 22:00 to 7:00 (Greathouse et al., 2017).

This study focuses on a new auroral feature observed in Jupiter's polar auroral region, characterized by circular H_2 emission patches expanding with time. The specifics about the UVS instrument and the observations used in this study are first presented, followed by the characterization of the newly observed auroral features. Finally, an interpretation and discussion of their potential origin is presented.

2. Instrument and Datasets

UVS is a photon-counting imaging spectrograph sensitive to the 68–210 nm spectral range, covering the major emission bands of Jupiter's UV auroras (Gladstone et al., 2017). Details about the instrument characterization and calibration are provided in previously published works (Davis et al., 2011; Greathouse et al., 2013; Hue et al., 2019a). UVS operates in scanning mode, imposed by Juno's spin period of 30 s. The nominal field-of-view of UVS is a 7.2°-long slit oriented along Juno's spin axis and centered on its spin plane. Thus, in a given spin of the spacecraft, UVS maps out a $360^\circ \times 7.2^\circ$ swath on the sky. The addition of a scan mirror allows UVS to shift the instrument field of view by up to $\pm 30^\circ$ above or below the spacecraft spin plane, giving UVS access to half of the sky at any given moment.

During a PJ observation period, which usually runs from -5 to $+5$ h with respect to the closest approach time, Juno's distance to Jupiter center ranges from $7 R_J$ down to $1.05 R_J$ at PJ. The angular size of Jupiter as seen by Juno ranges from $\sim 15^\circ$ – 150° . As Juno moves closer to the planet, UVS only gets a narrow swath of Jupiter's aurora each spin, and numerous scan mirror pointings are needed to cover the auroras entirely. It typically takes ~ 40 spins (20 min) of co-added observations using a large set of mirror pointings to produce a full image of Jupiter's auroras at a range of $1.6 R_J$. This also means that the temporal resolution on any single one point is at best ~ 30 s (i.e., one spin).

Most of the previous works using UVS data have exploited co-added swaths of data, and have focused on the global morphology and brightness of various auroral features (e.g. Bonfond et al., 2017, 2018, 2020; Clark et al., 2018; Gérard et al., 2018, 2020; Gladstone et al., 2017; Hue et al., 2019b; Mauk et al., 2017a). Other studies aimed at comparing UVS observations with simultaneous in situ particle measurements (Ebert et al., 2019; Gérard et al., 2019).

This work focuses on studying temporally evolving auroral features on a spin-by-spin basis, that is, 30 s apart. As Juno gets closer to PJ, the field of view of UVS on Jupiter becomes narrower. In addition to this, the pointing strategy changes on a PJ to PJ basis depending on the ever changing spacecraft/planet geometry. Observational strategies include: quick scans of the main aurora, scans at the satellite footprints and scanning at Juno's magnetic footprint. Therefore, not all PJs are identically suitable for detecting auroral features evolving on a \sim minute timescale. More specifically, from PJ1 until PJ23, Jupiter's northern aurora gets increasingly less visible because of Juno's orbital precession, while also bringing the spacecraft deeper into the radiation belts where the signal-to-noise ratio (SNR) is strongly decreased due to penetrating radiation. Additionally, Jupiter's orbital revolution causes Juno's inertially fixed orbital plane to change from an almost dawn-dusk configuration for PJ1 to a noon-midnight configuration for PJ23. To mitigate this, the pointing strategy in the north has been to perform quick scans across the aurora, in order to capture the overall morphology. The drawback of this approach is that it provides limited possibilities to perform temporal studies over the northern hemisphere, a situation that most likely will not improve moving forwards, as Juno will be dipping deeper into the northern radiation horn over time.

3. Feature Characterization

3.1. Spectral Characterization

Typical examples of the newly discovered expanding-ring features are presented in Figures 1 and 2, which show observations from PJ4 to PJ6, respectively. Panel A shows a single spin worth of data as view from Juno's vantage point, with the direction of the sun indicated by an orange arrow. The features evolve from an unresolved patch of emission, up to a $\sim 2,000$ km-wide elliptical ring of emission over the course of 3–4 spins (i.e., ~ 1.5 – 2 min). Details on the 4 best examples of the features recorded from PJ1 (August 27, 2016) up to PJ25 (February 17, 2020) are provided in Table 1. The spatial resolution at nadir corresponds to the instrument point spread function (PSF) projected on the planet, for a nadir-looking direction. Panel B displays the evolution of the features between subsequent spins, with a grid overlaid showing the distance with respect to the center of the emission. An ellipse was fitted to the emission pattern when the overall feature size is significantly larger than the instrument PSF.

The distribution of brightness of each pixel within the region of interest is presented on panels C. The region of interest is taken as the size of the ellipse plus twice the size of a single pixel (~ 100 – 200 km depending on

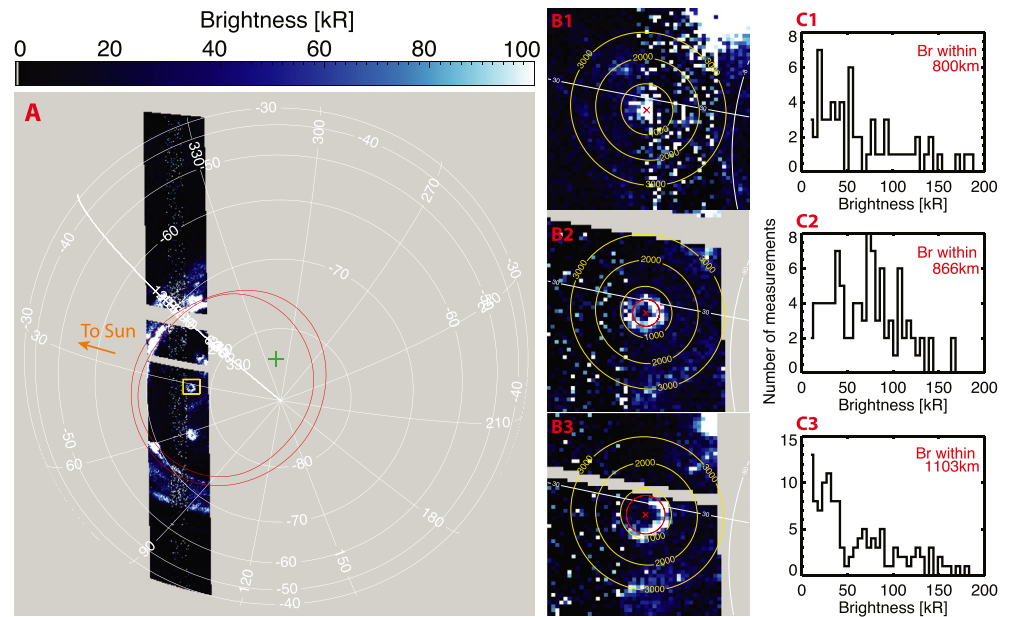


Figure 1. New feature detected on February 2, 2017 from 13:55:22 to 13:56:23, during PJ4 in the southern polar auroral region. Panel A: overview of the detected auroral emission over a single Juno-UVS swath, as viewed from Juno's vantage point. The yellow rectangle highlights the location of the feature, the orange arrow the direction of the sun at the time of the detection, and the reference ovals are from Bonfond et al. (2012). The green cross represents the sub-Juno position at the median detection time. Panel B: Evolution of the detected feature over consecutive Juno spins, as zoomed in the region highlighted by panel A's yellow rectangle. The red cross indicates the center of the feature, while the yellow contours shows the distance of every pixel to the center of the feature. Contours of 1,000, 2,000, and 3,000 km are shown on panels B. An ellipse fit (red ellipse) is performed on sub-panels B2 and B3, and the brightness histogram distribution of all pixels along the fitted ellipse is shown on sub-panels C2 and C3. No simultaneous Juno in situ measurements are available at the time this feature was detected.

the spacecraft altitude), in order to encompass all the emission coming from that feature while excluding the nearby emission. When no ellipse could be fitted, that is, when the feature is just forming and/or when the spatial resolution does not allow the identification of a circular feature, the brightness distribution was nominally calculated over a distance of 800 km, sufficiently large to encompass all the emission coming from the feature.

The brightnesses were calculated using the method presented by Hue et al. (2019b), that is using the photons recorded in the 115–118 nm and 125–165 nm range, and multiplied by 1.84 to extrapolate the brightness over the total H₂ and Lyman- α emissions, in the 75–198 nm range, and using aH₂ synthetic spectrum from Gustin et al. (2013). Another method to calculate the auroral UV-brightnesses was proposed by Bonfond et al. (2018) and Gérard et al. (2019), and used in subsequent papers (e.g., Allegrini et al., 2020; Szalay et al., 2020), which consists in using the photons recorded in the unabsorbed part of the spectrum (155–162 nm), multiplied by 8.1 to extrapolate over the entire Jovian H₂ spectrum, also using the spectrum of Gustin et al. (2013). Although the method proposed by Bonfond et al. (2018) is preferable because it allows calculating the UV-brightness consistently across auroral regions with significantly different color ratios, the method applied here was chosen to optimize the SNR over single spin of data by accumulating the maximum number of detected photons.

The brightness of the auroral features, as measured over consecutive spins, stays fairly constant over time, with intensities <140 kR. Because the brightness stays fairly constant, the integrated emitted power increases over time as the emitted surface increases. The total emitted power, as calculated following Hue et al. (2019b), increases from 0.17 to 0.21 GW for the PJ4 event and from 0.07 to 0.28 GW for the PJ6 event. The total emitted power of the PJ9 and PJ12 events increase from 0.05 to 0.13 GW and 0.04 to 0.07 GW respectively. One important observation is that the brightness distribution is rarely uniform along the ellipse. The emission of some part of the ellipse appears missing or significantly non-uniform (e.g., panels B3 and

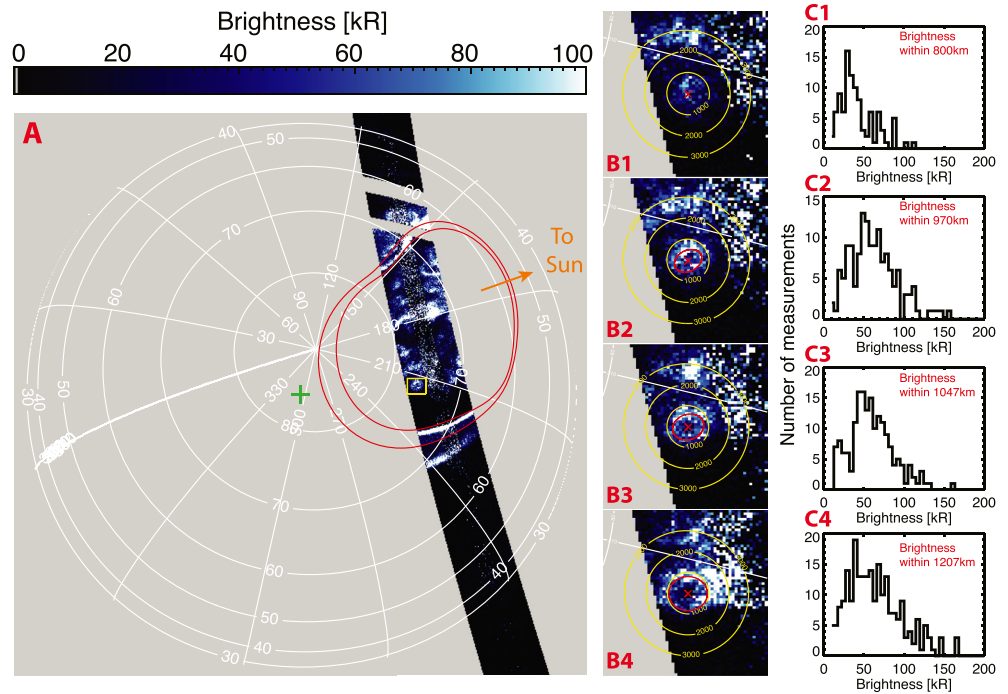


Figure 2. Same as Figure 1 for a feature detected on May 19, 2017 from 05:06:48 to 05:08:49 during PJ6 in the northern polar auroral region. No simultaneous Juno in situ measurements are available at the time this feature was detected.

B4 of Figures 1 and 2, respectively). The different features reported here evolve over 3–5 consecutive spins and vanish in various ways. In the PJ4 case, the feature terminates in the large diffuse patch of auroral emission, not entirely caught by UVS as the instrument pointing changed, targeting a neighboring region adjacent to the feature. The PJ6 and PJ9 features expand until they vanish in the auroral emission background. Note that the PJ6 feature shows a slight apparent warping, unlikely due to geometrical effects since the emission angle of that feature as seen by UVS varies from 25.4° to 25.9°. On the PJ12 event, the UVS pointing changed while the feature was observed, preventing the observation of the feature disappearance.

The evolution of the ellipse sizes for the best cases described above are presented in Figure 3A. The uncertainty of the fitted ellipse was taken as the size a single pixel (~100–200 km). The measured expansion rate of the features ranges from 3.3 ± 1.7 up to 7.7 ± 3.5 km/s. The occurrence rate for these events can be calculated assuming these derived properties and considering the amount of time the aurora has been observed by Juno-UVS. In the north, the occurrence rate ranges from 1.4 to 2.6 events per Jovian day, while in the south it ranges from 3.4 to 3.9 events per Jovian day (see supporting information for further details). The altitude at which these features originate is estimated by measurements of the color ratio, calculated as the ratio between the measured brightness in the 155–162 nm range over the one measured in the 125–130 nm range (Yung et al., 1982). Higher color ratio means emission coming from deeper in the atmosphere because

Table 1
Summary of the Best Examples of the Newly Detected Auroral Feature

Perijove	Hemisphere	Date	Start-stop time (UTC)	Subsolar Longitude [°]	Emission Angle [°]	Altitude [R_J]	Spatial resolution At nadir [km]	Figure
PJ4	S	February 02, 2017	13:55:22–13:56:23	26.2	21.7–21.0	1.17–1.19	294	Figure 1
PJ6	N	May 19, 2017	05:06:48–05:08:49	175.5	25.4–25.9	1.07–1.02	261	Figure 2
PJ9	N	October 24, 2017	17:06:02–17:07:33	263.0	24.3–22.5	0.65–0.62	158	Supporting information
PJ12	N	April 01, 2018	09:07:46–09:09:18	137.0	31.3–32.9	0.68–0.65	167	Supporting information

Note. Longitudes are in the System III and measured west.

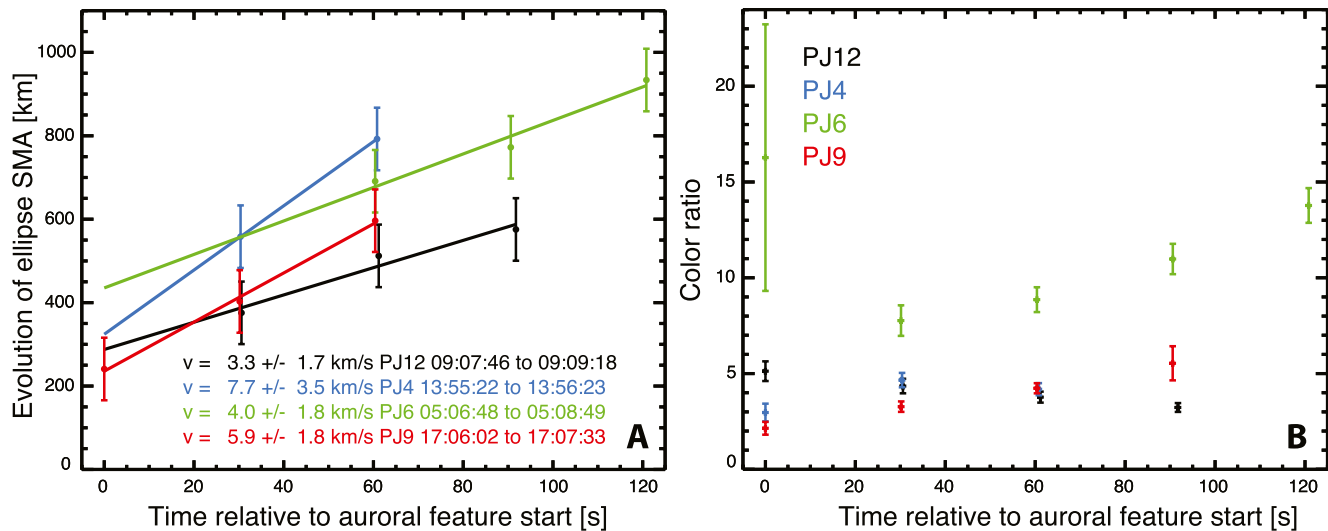


Figure 3. Panel A: Evolution of the ellipses semi major axes (SMA) sizes (km) for the auroral feature listed in Table 1. The expansion rates of each feature is derived and range from 3.3 ± 1.7 up to 7.7 ± 3.5 km/s. Panel B: evolution of the color ratios integrated over the area of the feature.

there is more atmospheric methane absorption. A color ratio increasing over time suggest the emission depth increases as well. Figure 3B shows the color ratio measured over the different features discussed above. Due to the low SNR obtained from single swaths worth of data over these features, the color ratio was calculated over the entire area that the brightness distribution was calculated on panels C of Figures 1 and 2. The measured color ratios range from ~ 3 to 15, when disregarding the low-SNR measurements recorded during the first swaths of the PJ9 and PJ12 cases. The mean color ratio as measured on the PJ4, PJ9, and PJ12 cases is 3.95. It is worth noting here that the feature recorded on PJ6 was located further inside the high-color ratio swirl region, as discussed in Section 3.2.

The color ratio can be used as an estimate of the mean energy of auroral electrons producing the auroral emission, provided the atmospheric structure of Jupiter is well-known. The more energetic, the deeper the electron penetration, and therefore the more absorbed intensity at $\lambda < 155$ nm from stratospheric methane producing a higher color ratio. Depending on the assumed atmospheric vertical structure (methane abundance and temperature profiles) and the electron transport method, the mean energy of auroral electrons deduced from the color ratio measurements may vary. Indeed, several studies using widely different methods determined that the methane homopause appears to be located at higher altitude in Jupiter's polar region relative to low-latitude regions, which leads to uncertainty in the derived emission altitude (Clark et al., 2018; Parkinson et al., 2006; Sinclair et al., 2019).

When considering the two-stream approach from previous studies (Gérard et al., 2003; Gustin et al., 2004, 2016), combined with the atmospheric models from Grodent et al. (2001) and Gladstone et al. (1996), a color ratio of 3.95 corresponds to a mean electron energy of 100 keV. Alternatively, the mono-energetic electron transport model by a Monte-Carlo method of Gérard et al. (2014) combined with the atmospheric models of Moses et al. (2005) predicts that mean electron energy in the range of 160–240 keV causes emission with color ratio of ~ 4 . The main differences between these methods are the assumed atmospheric model, as well as the method used for the electron transport. Following these approaches and given the uncertainties and assumption made in the modeling (atmospheric profile, vertical mixing efficiency, and electron transport method), the mean electron energy responsible for the auroral emissions presented here can be estimated to be ~ 80 –160 keV.

3.2. Magnetospheric Characterization

The magnetospheric origin of the presently described features is investigated here using the magnetic flux equivalence model of Vogt et al. (2011, 2015) to map back the origin of these features in Jupiter's magnetodisc. This model uses the Juno reference magnetic field model JRM09 that combines Juno's first 9 orbits

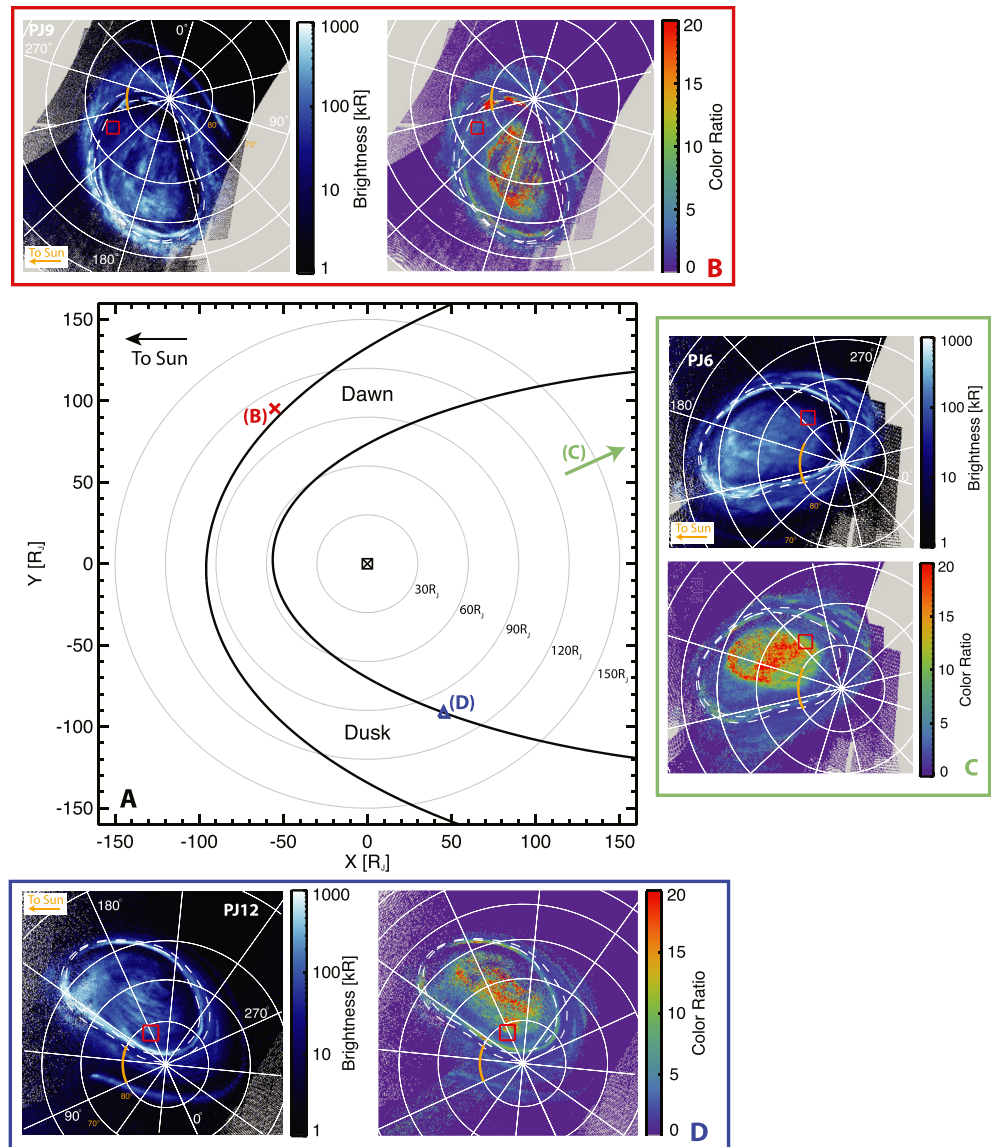


Figure 4. Panel A: equatorial view of Jupiter showing the location of the detected events, as mapped using the flux equivalence model of Vogt et al. (2011, 2015). The sun is located on the left toward negative X, the dawn-side magnetosphere at the top (positive Y) and the dusk-side magnetosphere at the bottom (negative Y). The magnetopause boundaries are shown using the empirical model of Joy et al. (2002). The colored crosses and arrows match panels B–D. Panels B–D: north polar projection showing averaged auroral emission (brightness and color ratio) during PJ9 (supporting information), PJ6 (Figure 2) and PJ12 (supporting information) respectively, using a larger integration window than for the circular expanding structure itself, allowing a full coverage over the entire aurora. The sun is located toward the left, similarly as panel A.

(Connerney et al., 2018). Figures 4 and 5 display the magnetospheric origin of these auroral features, in the north and in the south, respectively. The empirical formula of Joy et al. (2002) was used to display the magnetopause boundaries under two extreme states of the solar wind dynamical pressure.

Panels A on Figures 4 and 5 shows an equatorial cross section of Jupiter magnetosphere, with the sun on the left, and Jupiter at the origin, displayed by a crossed-square symbol. The position of the auroral feature, as mapped in that plane, are displayed using a color scheme matching the frame color of the additional panels (B–D). Panels B–D display polar projections of auroral brightnesses and color ratios associated with each event, using a larger time integration window around the detected time of the feature. Each panel is oriented such that the sun direction at the mid-time of the integration window is located toward the left

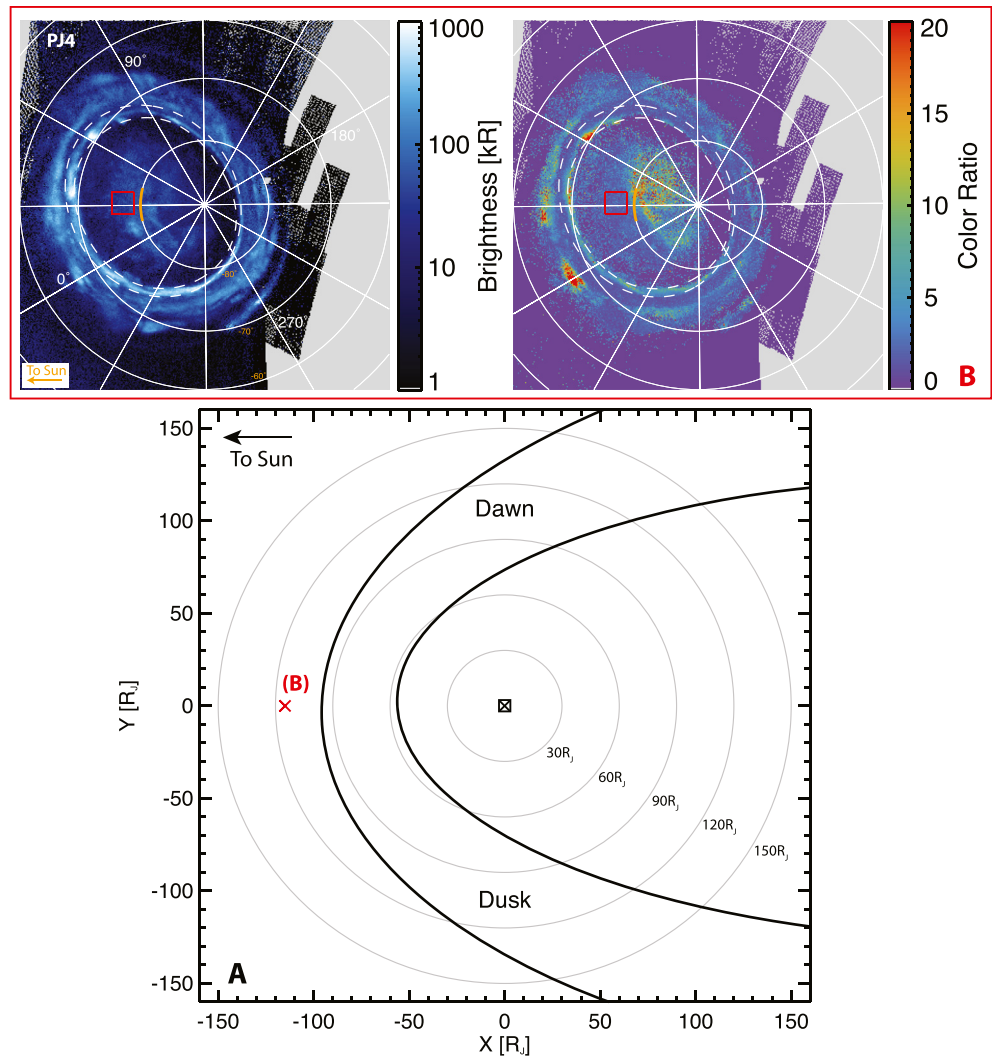


Figure 5. Same as Figure 4 for the feature detected in the South on PJ4.

hand-side of the plot. The orange semi-circle displayed along latitude of $\pm 80^\circ$ shows longitudinal direction of the sun over the entire time integration window used to make the maps. The location of the detected event is shown on each of the polar projections as red squares. The main oval reference position is used after Bonfond et al. (2012). The time range used to produce the averaged auroral image on Figures 4B–4D are October 24, 2017 16:25–17:15, May 19, 2017 04:00–05:32, and April 01, 2018 07:50–09:12, respectively. Data used to produce Figure 5B was recorded from February 02, 2017 13:38–14:27.

The Vogt et al. (2011, 2015) flux equivalence mapping, which was based on fits to magnetometer data from the Galileo spacecraft, becomes gradually unreliable as a function of magnetospheric distance. The data are limited to distances inside Galileo’s apoapsis ($\sim 150 R_J$ on the nightside) and inside the magnetopause on the dayside so the model validity is generally restricted to those regions. The PJ12 feature maps to distance of $102 R_J$ and local time (LT hereafter) of 19.8 hr. The features detected on PJ4, PJ6, and PJ9 map beyond the region of model validity, likely beyond the dayside magnetopause. However, it is possible to extend the Galileo data fit beyond the region of model validity to obtain a rough estimate (see supporting information for further details). Using this approach, the PJ4 and PJ9 events are estimated to map to $115 R_J$ near noon local time, and $100 R_J$ near 08:00 LT, respectively. In both cases these estimated distances are about $\sim 10\text{--}20 R_J$ beyond the region of model validity. The fit on the PJ12 event maps to an elliptical region in the magnetodisk

with characteristic semi-major axis ranging from $3.44 R_J$ to $6.64 R_J$. If that region is causing the emission, the potential source is expanding at a rate of up to $\sim 7,626$ km/s.

The PJ6 event, on the other hand, maps to a significantly different location than the other ones, and a similar method than presented by Haewsantati et al. (2020) was followed to retrieve an approximative magnetospheric local time of 1.7 hr. This method involves computing a straight line going from JRM09 magnetic pole (e.g., Connerney et al., 2018) to the auroral feature. Then, by extending that line toward the main oval, the magnetic local time was assigned to the first instance where the flux equivalence model maps within $150 R_J$. In this case, the LT direction is displayed as an arrow on Figure 4 indicating the magnetospheric local time. Note that this method does not account for the bend back of the magnetic field in the outer magnetosphere and therefore its results should be considered cautiously.

All detected events occur near the boundary between the high-color ratio region of the swirl region and the polar collar, as defined by Greathouse et al. (2017), a low color ratio region located between the main auroral and the swirl region that is devoid of bright auroral emission and that encompasses the previously defined UV active region and IR rotating dark polar region (r-DPR, see Section 4). Note that the color ratio of the PJ6 event appears significantly different from the other events, which could be due to either contamination from neighboring, high-color ratio, background, or because the atmosphere where the emissions occur is different than where the others occur (see Figure 4).

4. Interpretation

The processes responsible for these features have to produce the following observables:

1. Expanding ring of constant and moderately bright (<140 kR) UV emission
2. Mean color ratio integrated over the feature of ~ 3.95 not significantly evolving over time
3. Expansion rate of 3.3 ± 1.7 km/s up to 7.7 ± 3.5 km/s

Unfortunately, no simultaneous in situ measurements are available at the time these features were detected. Repeated measurements by Juno's particle instruments over the polar auroral region however provide a characteristic view of the particle populations connected to this region. Upward-directed electron beams are always seen by Juno over a large fraction of the polar region (Mauk et al., 2017b, 2020). In most cases, the energy distribution of these beams is broad and covers the JEDI energy range (~ 30 keV–1 MeV), sometimes up to the MeV range (Paranicas et al., 2018), and result from broadband acceleration processes. In some cases, coherent electrostatic potential structures create upward directed inverted-V type electron distribution profiles that are narrower in energy (Clark et al., 2017), occasionally peaking at energies down to several 10 s of keV (Ebert et al., 2017), as recorded by Juno's Jovian Auroral Distributions Experiment (JADE, McComas et al., 2017). Bi-directional beams of upgoing and downgoing electrons exhibiting power-law like distributions in energy have also been detected with energies extending up to several 10 s of keV and even up to ~ 100 keV (Ebert et al., 2017). These electron beams have the intriguing property of having the upward energy flux almost always greater than the downward energy flux. JEDI also revealed downward electrostatic potentials in the megavolt range as a very common feature in the polar auroral region, characterized by downward ion inverted-Vs (Clark et al., 2017; Mauk et al., 2020).

Assuming a conversion factor between UV brightness and electron energy flux of 10 kR corresponding to 1 mWm^{-2} (Grodent et al., 2001), the precipitating electron flux responsible for the feature described here should be around 10–15 mWm^{-2} . In addition, the color ratio measurements correspond to precipitating electrons in the energy range of 80–160 keV. JADE and JEDI previously recorded in situ measurements when connected to auroral emission patches of comparable UV brightness to the one described here (100–150 kR) (Ebert et al., 2019). They recorded upward going (i.e., away from Jupiter) electron fluxes that could be sufficient to cause these emissions. During the single PJ5 polar auroral crossing, Ebert et al. (2019) showed that most of the downward electron fluxes recorded by JADE peaked around $\sim 0.4 \text{ mWm}^{-2}$, and only a minor fraction (0.2%–0.3%) of the total downward fluxes lies in the 10–15 mWm^{-2} range. They interpreted the rarity of similarly important magnitude downward going electron fluxes in these regions as a likely consequence of the electron acceleration being located further down the magnetic field line toward the planet, assuming current closure.

G erard et al. (2019) converted the recorded UV emission from UVS at the footprint of Juno into an equivalent electron precipitation flux, and compared it to the JEDI measurements of energetic electron in the loss cone over the polar auroral regions. They found numerous cases with a systematic deficit in precipitating electron flux needed to explain the corresponding UV brightness, and fewer cases where the JEDI flux agrees with the diffuse polar auroral brightness. They noted that these numbers could only be compared when no acceleration mechanisms are located further down the field line toward the planet. The current theories for the electron acceleration processes imply an acceleration region located at an altitude of $\sim 0.5\text{--}1.5 R_J$, which is, at times, compatible with the range of altitude Juno was at over the polar aurora. G erard et al. (2019) concluded that Juno might have flown below, inside or above the electron acceleration region during the time of the comparison, explaining the partial agreement.

Precipitating electron populations in the energy range of 80–160 keV observed at energy flux of 10–15 mW m^{-2} have only been rarely observed to date by Juno’s charged particle instrument suite over the polar auroral region. In situ instruments on Juno showed the predominance of broadband acceleration processes generating upward electron beams. So far, Juno has seemingly almost always been located above the region where this acceleration takes place, and the JEDI measurements suggest that, for a fraction of all recorded PJ polar auroral crossing, the downward acceleration counterpart of that beam appears at lower altitudes (Mauk et al., 2020). The current thinking is that they could be generated by: (i) the magnetically reflected component of the upward beams; (ii) the consequence of beams generated from the opposite hemisphere; or (iii) the evidence for associated local acceleration as Juno dips into a broad acceleration region at lower altitudes. One could therefore argue that these downward beams are responsible for the features discussed here. If this is the case, more dedicated studies are needed to characterize them.

Moreover, one could argue that the transient UV features discussed here might be caused by the downward counterpart of the transient upward electron inverted-Vs, characterized by peaked energy distribution and detected in the polar region (Clark et al., 2017). Two main issues also hamper that origin: (i) these downward electron inverted Vs have not been observed yet, (ii) one would expect them to cause a distinct auroral signature, characterized by higher color ratio at the center of the feature and lower at the edges, which UVS does not support observationally.

Several important observations can be made from this analysis. First, the feature discussed here is located on the edges of the UV swirl region. The swirl region was previously associated with the IR fixed Dark Polar Region (f-DPR). Second, as shown in Figures 4 and 5, the observed features map to distant regions in the magnetosphere ($>100R_J$). Dayside pulsed reconnections occurring near Jupiter’s magnetopause was previously associated with the generation of the polar auroral UV spot and X-rays (Bunce et al., 2004). These reconnection events lead to vortical flows in the magnetosphere and ionosphere, supposedly located in the boundary region between the close/open field lines, and give rise to pulsed bipolar field-aligned currents. Bunce et al. (2004) suggested that the reconnection pulses should be characterized by two adjacent spots and arcs of UV emission of the order of few 1,000 km along that boundary, and 100 km wide, with centers separated by several 1,000 s km. They concluded that reconnection phenomena should be more active under higher solar wind density. Under slower solar wind condition, they estimated typical brightnesses peaking at ~ 400 kR for the auroral signatures located in the closed field line region. The typical brightnesses measured over the feature discussed here are about the right order of magnitude than predicted from a dayside reconnection under slow solar wind condition. However, the morphology of the feature seems fairly different than the one expected from dayside reconnection, showing an expanding circular emission pattern instead of the predicted spot and arc.

Additionally, Haewsantati et al. (2020) reported observing transient spots in Jupiter’s polar auroral region using Juno-UVS, also located near the edge of the swirl region, and occasionally pulsating or occurring repetitively with periodicities slightly longer ($\sim 20\text{--}30$ minutes) than previously identified quasi-periodic flares ($\sim 2\text{--}5$ minutes) (Bonfond et al., 2016, 2011; Nichols et al., 2017b). Although reported in similar region within the polar aurora as the features discussed here, the difference in morphology, typical brightness, feature growth as well as periodic behavior suggest a different origin. They found these repetitive spots to corotate with Jupiter, ruling out their potential noon-facing magnetospheric cusp-related origin, although the non-trivial magnetic field topology in that region might complicate the picture (Zhang et al., 2020).

The discovery of a type of aurora on Earth also showing concentrically expanding ring-shaped emission features was recently presented (Hosokawa et al., 2020). These auroras were found in the context of more generally pulsating aurora, which are thought to be correlated with the periodic appearing of chorus waves in the magnetosphere (Ozaki et al., 2018). When mapped to the Earth magnetosphere, these chorus waves may have been generated by a source expanding at a velocity of $\sim 1,000$ km/s (Hosokawa et al., 2020). At Jupiter, chorus waves and hiss emissions are thought to be mainly responsible for the scattering and loss of trapped electrons (e.g., Gurnett & Scarf, 1983), and have been observed in the inner magnetosphere by Galileo (Menietti et al., 2016), and more recently by the WAVES instrument (Kurth et al., 2017) on Juno (Li et al., 2020). At larger distances, in the plasma sheet boundary layer, Juno witnessed a strong wave activity (Zhang et al., 2020). These could be generated by high-energy field-aligned electrons, although the electron field-aligned anisotropy observed there suggest a different mechanism instead. Upward propagating electron beams were also detected in correlation with broadband auroral hiss whistler mode waves on Juno (Tetrick et al., 2017). These upward propagating waves may significantly interact with the upward beam of electrons, causing them pitch-angle and energy scattering (Elliott et al., 2018), and intense upward-propagating whistler mode waves can be generated by upgoing electron beams via Landau resonance (Elliott et al., 2020). Again, no simultaneous in situ or WAVES measurements were available at the times of the detection.

Viscous processes at the magnetopause due to the interaction between the high Alfvén Mach number from the solar wind with the high- β magnetospheric plasma may be important mechanisms to transport mass and momentum across the magnetopause. These interactions would allow intermittent magnetic reconnection in the region of interaction (Delamere & Bagenal, 2010). One type of instability that might be generated in the region of viscous interaction is the Kelvin-Helmholtz (KH) instability, in which the magnetic field lines get twisted. In these regions, models predict strong field-aligned current bounding the KH vortices (Delamere et al., 2013; Nakamura et al., 2011). On Saturn, the shear flows on the prenoon dayside magnetopause is expected to be more pronounced than the postnoon sector due to the rapid rotation of the corotating magnetodisk, which makes it more KH unstable. Modeling shows that KH vortices generated in the subsolar region are then transported into the postnoon sector (Ma et al., 2015). Additionally, high-latitude dayside reconnection has also been proposed and debated as the dominant reconnection process at Jupiter (Cowley et al., 2008; McComas & Bagenal, 2007, 2008). In this scenario, and because of the size of the Jovian magnetosphere, its rapid rotation and internal sources of plasma, lobe reconnection is expected to occur at high latitudes instead of the open field lines being dragged down in the magnetotail and reconnecting following a Dungey-cycle. This concept is still subject of debate (e.g., Delamere et al., 2015).

Based on the location in the magnetodisk where these event are seen from, a KH instabilities origin remains a strong candidate to explain some of the features discussed here. Further studies dedicated to the morphological auroral UV signatures resulting from the field-aligned current bounding a region of KH vortices or following a dayside reconnection are needed to conclude on the origin of the newly discovered features.

5. Summary

This paper describes the analysis of a new auroral feature discovered in the Juno-UVS datasets, which consists of circular emission patches seen in Jupiter's polar auroral region. Due to observational constraints, it can only be detected using consecutive swaths of UVS data recorded over the same region, which were recorded ~ 30 s apart. The feature expands into an elliptically shaped patch of moderately-bright emission (< 140 kR) in terms of total H_2 and Lyman- α emissions in the 75–198 nm range. It grows until the ellipse reaches a semi-major axis size of $\sim 1,000$ km, and then either merges with nearby auroral patches, dims away to lower brightness, or dissipates in a diffuse patch of auroral emission.

Due to the rapidly changing spatial resolution of UVS over the course of a perijove, only a set of four features were distinct enough to proceed to further analysis. Three were measured in the north and one in the south, and were recorded over four different perijove datasets (PJ4, PJ6, PJ9, and PJ12). Measurement of the feature's expansion rate proved challenging owing to the low SNR of single spins of UVS data on moderately-bright UV emission patches. The expansion measured over these four best cases ranged from 3.3 ± 1.7 up to 7.7 ± 3.5 km/s.

The time-averaged color ratio integrated over the entire elliptical region is ~ 3.95 , and no strong temporal dependence of the color ratio was found despite the low statistics. The mean energy of auroral electrons inverted from emission with such color ratio is in the 80–160 keV range, as inferred from previously developed models of Gérard et al. (2014) and Gustin et al. (2016). This suggests a fairly constant energy of the precipitating particles triggering these events, as both the brightness and the color ratio appear steady over time.

Using the magnetic flux mapping of Vogt et al. (2011), these events map in the magnetodisk at distance $> 100 R_J$. The northern auroral features map to magnetospheric local times of 12, 8 and 19.8 hr, while the southern one maps to magnetospheric local time of 1.7 hr. Field-aligned current associated with pulsed dayside magnetopause reconnection have previously been associated with the generation of pulsed UV spots and X-rays (Bunce et al., 2004; Dunn et al., 2017). Kelvin-Helmholtz instabilities associated with shear flows near the magnetopause is also expected to generate field-aligned current potentially triggering UV-spot emissions in the polar auroral region (Delamere & Bagenal, 2010). It seems these two processes are most likely the drivers for the observed emissions, but further modeling and observational data is needed to come to a clear conclusion.

Data Availability Statement

All the data used in this study are publicly available on the PDS Atmospheres Node Data Set Catalog (https://pds-atmospheres.nmsu.edu/cgi-bin/getdir.pl?dir=DATA&volume=jnouv_3001).

Acknowledgments

The authors are grateful to NASA and contributing institutions that have made the Juno mission possible. The Ultraviolet Spectrograph (UVS) work was funded by NASA's New Frontiers Program for Juno via a subcontract with Southwest Research Institute. Juno operations are supported by NASA (managed by the Jet Propulsion Laboratory). B. Bonfond, J.-C. Gerard, and D. C. Grodent acknowledge funding for this research by a PRODEX contract of ESA, managed with the help of BELSPO. The authors thank Leo Gkouvelis for providing a conductance model outputs. The authors would like to thank Sadie Elliott, Hunter Waite and Wen Li, as well as our two reviewers for helpful comments and discussions.

References

- Allegrini, F., Mauk, B., Clark, G., Gladstone, G. R., Hue, V., Kurth, W. S., et al. (2020). Energy flux and characteristic energy of electrons over Jupiter's main auroral emission. *Journal of Geophysical Research: Space Physics*, *125*(4), e27693. <https://doi.org/10.1029/2019JA027693>
- Badman, S. V., Branduardi-Raymont, G., Galand, M., Hess, S. L. G., Krupp, N., Lamy, L., et al. (2015). Auroral processes at the giant planets: Energy deposition, emission mechanisms, morphology and spectra. *Space Science Reviews*, *187*(1–4), 99–179. <https://doi.org/10.1007/s11214-014-0042-x>
- Bonfond, B., Gladstone, G. R., Grodent, D., Gérard, J. C., Greathouse, T. K., Hue, V., et al. (2018). Bar code events in the Juno-UVS Data: Signature ~ 10 MeV electron microbursts at Jupiter. *Geophysical Research Letters*, *45*(22), 108–112. <https://doi.org/10.1029/2018GL080490>
- Bonfond, B., Gladstone, G. R., Grodent, D., Greathouse, T. K., Versteeg, M. H., Hue, V., et al. (2017). Morphology of the UV aurorae Jupiter during Juno's first perijove observations. *Geophysical Research Letters*, *44*, 4463–4471. <https://doi.org/10.1002/2017GL073114>
- Bonfond, B., Grodent, D., Badman, S. V., Gérard, J.-C., & Radioti, A. (2016). Dynamics of the flares in the active polar region of Jupiter. *Geophysical Research Letters*, *43*(23), 11963–11970. <https://doi.org/10.1002/2016GL071757>
- Bonfond, B., Grodent, D., Gérard, J.-C., Stallard, T., Clarke, J. T., Yoneda, M., et al. (2012). Auroral evidence of Io's control over the magnetosphere of Jupiter. *Geophysical Research Letters*, *39*(1), L01105. <https://doi.org/10.1029/2011GL050253>
- Bonfond, B., Vogt, M. F., Gérard, J.-C., Grodent, D., Radioti, A., & Coumans, V. (2011). Quasi-periodic polar flares at Jupiter: A signature of pulsed dayside reconnections?. *Geophysical Research Letters*, *38*(2), L02104. <https://doi.org/10.1029/2010GL045981>
- Bonfond, B., Yao, Z., & Grodent, D. (2020). Six pieces of evidence against the corotation enforcement theory to explain the main aurora at Jupiter. *Journal of Geophysical Research: Space Physics*, *125*(11), e2020JA028152.
- Branduardi-Raymont, G., Elsner, R. F., Galand, M., Grodent, D., Cravens, T. E., Ford, P., et al. (2008). Spectral morphology of the X-ray emission from Jupiter's aurorae. *Journal of Geophysical Research*, *113*(A2), A02202. <https://doi.org/10.1029/2007JA012600>
- Bunce, E. J., Cowley, S. W. H., & Yeoman, T. K. (2004). Jovian cusp processes: Implications for the polar aurora. *Journal of Geophysical Research*, *109*(A9), A09S13. <https://doi.org/10.1029/2003JA010280>
- Clarke, J. T., Grodent, D., Cowley, S. W. H., Bunce, E. J., Zarka, P., Connerney, J. E. P., & Satoh, T. (2004). *Jupiter's Aurora*. In B. Fran, E. D. Timothy, B. M. William (Eds.), *Jupiter. The planet, satellites and magnetosphere*. (Vol. 1, pp. 639–670).
- Clark, G., Mauk, B. H., Haggerty, D., Paranicas, C., Kollmann, P., Rymer, A., et al. (2017). Energetic particle signatures of magnetic field-aligned potentials over Jupiter's polar regions. *Geophysical Research Letters*, *44*(17), 8703–8711. <https://doi.org/10.1002/2017GL074366>
- Clark, G., Tao, C., Mauk, B. H., Nichols, J., Saur, J., Bunce, E. J., et al. (2018). Precipitating electron energy flux and characteristic energies in Jupiter's main auroral region as measured by Juno/JEDI. *Journal of Geophysical Research: Space Physics*, *123*(9), 7554–7567. <https://doi.org/10.1029/2018JA025639>
- Connerney, J. E. P., Adriani, A., Allegrini, F., Bagenal, F., Bolton, S. J., Bonfond, B., et al. (2017). Jupiter's magnetosphere and aurorae observed by the Juno spacecraft during its first polar orbits. *Science*, *356*(6340), 826–832. <https://doi.org/10.1126/science.aam5928>
- Connerney, J. E. P., Kotsiaros, S., Oliverson, R. J., Espley, J. R., Joergensen, J. L., Joergensen, P. S., et al. (2018). A new model of Jupiter's magnetic field from Juno's first nine orbits. *Geophysical Research Letters*, *45*, 2590–2596. <https://doi.org/10.1002/2018GL077312>
- Cowley, S. W. H., Badman, S. V., Imber, S. M., & Milan, S. E. (2008). Comment on "Jupiter: A fundamentally different magnetospheric interaction with the solar wind" by D. J. McComas and F. Bagenal. *Geophysical Research Letters*, *35*(10), L10101. <https://doi.org/10.1029/2007GL032645>
- Cowley, S. W. H., Bunce, E. J., Stallard, T. S., & Miller, S. (2003). Jupiter's polar ionospheric flows: Theoretical interpretation. *Geophysical Research Letters*, *30*(5), 1220. <https://doi.org/10.1029/2002GL016030>
- Davis, M. W., Gladstone, G. R., Greathouse, T. K., Slater, D. C., Versteeg, M. H., Persson, K. B., et al. (2011). Radiometric performance results of the Juno ultraviolet spectrograph (Juno-UVS). *Society of Photo-Optical Instrumentation Engineers (SPIE) Conference Series*, *8146*. 814604. <https://doi.org/10.1117/12.894274>
- Delamere, P. A., & Bagenal, F. (2010). Solar wind interaction with Jupiter's magnetosphere. *Journal of Geophysical Research*, *115*(A10), A10201. <https://doi.org/10.1029/2010JA015347>

- Delamere, P. A., Bagenal, F., Paranicas, C., Masters, A., Radioti, A., Bonfond, B., et al. (2015). Solar wind and internally driven dynamics: Influences on magnetodiscs and auroral responses. *Space Science Reviews*, 187(1–4), 51–97. <https://doi.org/10.1007/s11214-014-0075-1>
- Delamere, P. A., Wilson, R. J., Eriksson, S., & Bagenal, F. (2013). Magnetic signatures of Kelvin-Helmholtz vortices on Saturn's magnetopause: Global survey. *Journal of Geophysical Research: Space Physics*, 118(1), 393–404. <https://doi.org/10.1029/2012JA018197>
- Dungey, J. W. (1961). Interplanetary magnetic field and the auroral zones. *Physical Review Letters*, 6, 47–48. <https://doi.org/10.1103/PhysRevLett.6.47>
- Dunn, W. R., Branduardi-Raymont, G., Ray, L. C., Jackman, C. M., Kraft, R. P., Elsner, R. F., et al. (2017). The independent pulsations of Jupiter's northern and southern X-ray auroras. *Nature Astronomy*, 1, 758–764. <https://doi.org/10.1038/s41550-017-0262-6>
- Ebert, R. W., Allegrini, F., Bagenal, F., Bolton, S. J., Connerney, J. E. P., Clark, G., et al. (2017). Spatial distribution and properties of 0.1–100 keV electrons in Jupiter's polar auroral region. *Geophysical Research Letters*, 44(18), 9199–9207. <https://doi.org/10.1002/2017GL075106>
- Ebert, R. W., Greathouse, T. K., Clark, G., Allegrini, F., Bagenal, F., Bolton, S. J., et al. (2019). Comparing electron energetics and UV brightness in Jupiter's northern polar region during Juno Perijove 5. *Geophysical Research Letters*, 46(1), 19–27. <https://doi.org/10.1029/2018GL081129>
- Elliott, S. S., Gurnett, D. A., Kurth, W. S., Mauk, B. H., Ebert, R. W., Clark, G., et al. (2018). The acceleration of electrons to high energies over the Jovian polar cap via whistler mode wave-particle interactions. *Journal of Geophysical Research: Space Physics*, 123(9), 7523–7533. <https://doi.org/10.1029/2018JA025797>
- Elliott, S. S., Gurnett, D. A., Yoon, P. H., Kurth, W. S., Mauk, B. H., Ebert, R. W., et al. (2020). The generation of upward-propagating whistler mode waves by electron beams in the Jovian polar regions. *Journal of Geophysical Research: Space Physics*, 125(6), e27868. <https://doi.org/10.1029/2020JA027868>
- Gérard, J.-C., Bonfond, B., Grodent, D., Radioti, A., Clarke, J. T., Gladstone, G. R., et al. (2014). Mapping the electron energy in Jupiter's aurora: Hubble spectral observations. *Journal of Geophysical Research: Space Physics*, 119(11), 9072–9088. <https://doi.org/10.1002/2014JA020514>
- Gérard, J. C., Bonfond, B., Mauk, B. H., Gladstone, G. R., Yao, Z. H., Greathouse, T. K., et al. (2019). Contemporaneous observations of Jovian energetic auroral electrons and ultraviolet emissions by the Juno spacecraft. *Journal of Geophysical Research: Space Physics*, 124(11), 8298–8317. <https://doi.org/10.1029/2019JA026862>
- Gérard, J. C., Gkouvelis, L., Bonfond, B., Grodent, D., Gladstone, G. R., Hue, V., et al. (2020). Spatial distribution of the Pedersen conductance in the Jovian aurora from Juno-UVS spectral images. *Journal of Geophysical Research: Space Physics*, 125(8), e28142. <https://doi.org/10.1029/2020JA028142>
- Gérard, J.-C., Gustin, J., Grodent, D., Clarke, J. T., & Grard, A. (2003). Spectral observations of transient features in the FUV Jovian polar aurora. *Journal of Geophysical Research*, 108(A8), 1319. <https://doi.org/10.1029/2003JA009901>
- Gérard, J.-C., Mura, A., Bonfond, B., Gladstone, G. R., Adriani, A., Hue, V., et al. (2018). Concurrent ultraviolet and infrared observations of the north Jovian aurora during Juno's first perijove. *Icarus*, 312, 145–156. <https://doi.org/10.1016/j.icarus.2018.04.020>
- Gladstone, G. R., Allen, M., & Yung, Y. L. (1996). Hydrocarbon photochemistry in the upper atmosphere of Jupiter. *Icarus*, 119(1), 1–52. <https://doi.org/10.1006/icar.1996.0001>
- Gladstone, G. R., Persyn, S. C., Eterno, J. S., Walther, B. C., Slater, D. C., Davis, M. W., et al. (2017a). The ultraviolet spectrograph on NASA's Juno mission. *Space Science Reviews*, 213, 447–473. <https://doi.org/10.1007/s11214-014-0040-z>
- Gladstone, G. R., Versteeg, M. H., Greathouse, T. K., Hue, V., Davis, M. W., Gérard, J.-C., et al. (2017b). Juno-UVS approach observations of Jupiter's auroras. *Geophysical Research Letters*, 44, 7668–7675. <https://doi.org/10.1002/2017GL073377>
- Greathouse, T. K., Gladstone, G. R., Davis, M. W., Slater, D. C., Versteeg, M. H., Persson, K. B., et al. (2013). Performance results from in-flight commissioning of the Juno Ultraviolet Spectrograph (Juno-UVS). *Proceedings of the SPIE*, 8859, 88590T. <https://doi.org/10.1117/12.2024537>
- Greathouse, T. K., Gladstone, G. R., Versteeg, M. H., Hue, V., Kammer, J., Davis, M. W., et al. (2017). A study of local time variations of Jupiter's ultraviolet aurora using Juno-UVS. AGU Fall Meeting Abstracts (Vol. 2017). P24A–07.
- Grodent, D. (2015). A brief review of ultraviolet auroral emissions on giant planets. *Space Science Reviews*, 187(1–4), 23–50. <https://doi.org/10.1007/s11214-014-0052-8>
- Grodent, D., Clarke, J. T., Waite, J. H., Cowley, S. W. H., Gérard, J. C., & Kim, J. (2003). Jupiter's polar auroral emissions. *Journal of Geophysical Research*, 108(A10), 1366. <https://doi.org/10.1029/2003JA010017>
- Grodent, D., Waite, J. H., & Gérard, J.-C. (2001). A self-consistent model of the Jovian auroral thermal structure. *Journal of Geophysical Research*, 106(A7), 12933–12952. <https://doi.org/10.1029/2000JA900129>
- Gurnett, D. A., & Scarf, F. L. (1983). *Physics of the Jovian magnetosphere. 8. Plasma waves in the Jovian magnetosphere*. (pp. 285–316). Cambridge University Press.
- Gustin, J., Feldman, P. D., Gérard, J.-C., Grodent, D., Vidal-Madjar, A., Ben Jaffel, L., et al. (2004). Jovian auroral spectroscopy with FUSE: Analysis of self-absorption and implications for electron precipitation. *Icarus*, 171(2), 336–355. <https://doi.org/10.1016/j.icarus.2004.06.005>
- Gustin, J., Grodent, D., Gérard, J. C., Radioti, A., Bunce, E. J., Nichols, J. D., & Clarke, J. T. (2013). Mapping of the Jovian auroral electron energy with HST/STIS observations. In *European Planetary Science Congress*. EPSC2013–596.
- Gustin, J., Grodent, D., Ray, L. C., Bonfond, B., Bunce, E. J., Nichols, J. D., & Ozak, N. (2016). Characteristics of north Jovian aurora from STIS FUV spectral images. *Icarus*, 268, 215–241. <https://doi.org/10.1016/j.icarus.2015.12.048>
- Haewasantati, K., Bonfond, B., Wannawichian, S., & Gladstone, G. R. (2020). Jupiter's polar auroral bright spots as seen by Juno-UVS. In *EGU General Assembly Conference Abstracts* (p. 3622). EGU General Assembly Conference Abstracts..
- Hosokawa, K., Kurita, S., Miyoshi, Y., Oyama, S.-I., Ogawa, Y., Kasahara, Y., et al. (2020). *Concentrically expanding ring-shaped pulsating aurora: Simultaneous observations with Arase and high-speed cameras in Scandinavia*. AGU Fall Meeting Abstracts (Vol. 2020). pp. SM001–03.
- Hue, V., Greathouse, T. K., Bonfond, B., Saur, J., Gladstone, G. R., Roth, L., et al. (2019b). Juno-UVS observation of the Io footprint during solar eclipse. *Journal of Geophysical Research: Space Physics*, 124(7), 5184–5199. <https://doi.org/10.1029/2018JA026431>
- Hue, V., Randall Gladstone, G., Greathouse, T. K., Kammer, J. A., Davis, M. W., Bonfond, B., et al. (2019a). In-flight Characterization and Calibration of the Juno-ultraviolet Spectrograph (Juno-UVS). *The Astronomical Journal*, 157(2), 90. <https://doi.org/10.3847/1538-3881/aafb36>
- Johnson, R. E., Stallard, T. S., Melin, H., Nichols, J. D., & Cowley, S. W. H. (2017). Jupiter's polar ionospheric flows: High resolution mapping of spectral intensity and line-of-sight velocity of H₃⁺ ions. *Journal of Geophysical Research: Space Physics*, 122(7), 7599–7618. <https://doi.org/10.1002/2017JA024176>

- Joy, S. P., Kivelson, M. G., Walker, R. J., Khurana, K. K., Russell, C. T., & Ogino, T. (2002). Probabilistic models of the Jovian magnetopause and bow shock locations. *Journal of Geophysical Research*, *107*(A10), 1309. <https://doi.org/10.1029/2001JA009146>
- Kivelson, M. G., & Southwood, D. J. (2005). Dynamical consequences of two modes of centrifugal instability in Jupiter's outer magnetosphere. *Journal of Geophysical Research*, *110*(A12), A12209. <https://doi.org/10.1029/2005JA011176>
- Kurth, W. S., Hospodarsky, G. B., Kirchner, D. L., Mokrzycki, B. T., Averkamp, T. F., Robison, W. T., et al. (2017). The Juno waves investigation. *Space Science Reviews*, *213*, 347–392. <https://doi.org/10.1007/s11214-017-0396-y>
- Li, W., Shen, X. C., Menietti, J. D., Ma, Q., Zhang, X. J., Kurth, W. S., & Hospodarsky, G. B. (2020). Global distribution of whistler mode waves in jovian inner magnetosphere. *Geophysical Research Letters*, *47*(15), e2020GL088198. <https://doi.org/10.1029/2020gl088198>
- Mauk, B. H., Clark, G., Gladstone, G. R., Kotsiaros, S., Adriani, A., Allegrini, F., et al. (2020). Energetic particles and acceleration regions over Jupiter's polar cap and main aurora: A broad overview. *Journal of Geophysical Research: Space Physics*, *125*(3), e27699. <https://doi.org/10.1029/2019JA027699>
- Mauk, B. H., Haggerty, D. K., Paranicas, C., Clark, G., Kollmann, P., Rymer, A. M., et al. (2017a). Discrete and broadband electron acceleration in Jupiter's powerful aurora. *Nature*, *549*(7670), 66–69. <https://doi.org/10.1038/nature23648>
- Mauk, B. H., Haggerty, D. K., Paranicas, C., Clark, G., Kollmann, P., Rymer, A. M., et al. (2017b). Juno observations of energetic charged particles over Jupiter's polar regions: Analysis of monodirectional and bidirectional electron beams. *Geophysical Research Letters*, *44*(10), 4410–4418. <https://doi.org/10.1002/2016GL072286>
- Ma, X., Stauffer, B., Delamere, P. A., & Otto, A. (2015). Asymmetric Kelvin-Helmholtz propagation at Saturn's dayside magnetopause. *Journal of Geophysical Research: Space Physics*, *120*(3), 1867–1875. <https://doi.org/10.1002/2014JA020746>
- McComas, D. J., Alexander, N., Allegrini, F., Bagenal, F., Beebe, C., Clark, G., et al. (2017). The Jovian auroral distributions experiment (JADE) on the Juno mission to Jupiter. *Space Science Reviews*, *213*(1–4), 547–643. <https://doi.org/10.1007/s11214-013-9990-9>
- McComas, D. J., & Bagenal, F. (2007). Jupiter: A fundamentally different magnetospheric interaction with the solar wind. *Geophysical Research Letters*, *34*(20), L20106. <https://doi.org/10.1029/2007GL031078>
- McComas, D. J., & Bagenal, F. (2008). Reply to comment by S. W. H. Cowley et al. on “Jupiter: A fundamentally different magnetospheric interaction with the solar wind”. *Geophysical Research Letters*, *35*(10), L10103. <https://doi.org/10.1029/2008GL034351>
- Menietti, J. D., Groene, J. B., Averkamp, T. F., Horne, R. B., Woodfield, E. E., Shprits, Y. Y., et al. (2016). Survey of whistler mode chorus intensity at Jupiter. *Journal of Geophysical Research: Space Physics*, *121*(10), 9758–9770. <https://doi.org/10.1002/2016ja022969>
- Moses, J. I., Fouchet, T., Bézard, B., Gladstone, G. R., Lellouch, E., & Feuchtgruber, H. (2005). Photochemistry and diffusion in Jupiter's stratosphere: Constraints from ISO observations and comparisons with other giant planets. *Journal of Geophysical Research*, *110*(E8), E08001. <https://doi.org/10.1029/2005JE002411>
- Nakamura, T. K. M., Hasegawa, H., Shinohara, I., & Fujimoto, M. (2011). Evolution of an MHD-scale Kelvin-Helmholtz vortex accompanied by magnetic reconnection: Two-dimensional particle simulations. *Journal of Geophysical Research*, *116*(A3), A03227. <https://doi.org/10.1029/2010JA016046>
- Nichols, J. D., Badman, S. V., Bagenal, F., Bolton, S. J., Bonfond, B., Bunce, E. J., et al. (2017a). Response of Jupiter's auroras to conditions in the interplanetary medium as measured by the Hubble Space Telescope and Juno. *Geophysical Research Letters*, *44*(15), 7643–7652. <https://doi.org/10.1002/2017GL073029>
- Nichols, J. D., Bunce, E. J., Clarke, J. T., Cowley, S. W. H., Gérard, J.-C., Grodent, D., & Pryor, W. R. (2007). Response of Jupiter's UV auroras to interplanetary conditions as observed by the Hubble Space Telescope during the Cassini flyby campaign. *Journal of Geophysical Research*, *112*(A2), A02203. <https://doi.org/10.1029/2006JA012005>
- Nichols, J. D., Clarke, J. T., Gérard, J. C., & Grodent, D. (2009b). Observations of Jovian polar auroral filaments. *Geophysical Research Letters*, *36*(8), L08101. <https://doi.org/10.1029/2009GL037578>
- Nichols, J. D., Clarke, J. T., Gérard, J. C., Grodent, D., & Hansen, K. C. (2009a). Variation of different components of Jupiter's auroral emission. *Journal of Geophysical Research*, *114*(A6), A06210. <https://doi.org/10.1029/2009JA014051>
- Nichols, J. D., Yeoman, T. K., Bunce, E. J., Chowdhury, M. N., Cowley, S. W. H., & Robinson, T. R. (2017b). Periodic emission within Jupiter's main auroral oval. *Geophysical Research Letters*, *44*(18), 9192–9198. <https://doi.org/10.1002/2017GL074824>
- Ozaki, M., Shiokawa, K., Miyoshi, Y., Hosokawa, K., Oyama, S., Yagitani, S., et al. (2018). Microscopic observations of pulsating aurora associated with chorus element structures: Coordinated arase satellite-PWING observations. *Geophysical Research Letters*, *45*(22), 12125–12134. <https://doi.org/10.1029/2018GL079812>
- Pallier, L., & Prangé, R. (2001). More about the structure of the high latitude Jovian aurorae. *Planetary and Space Science*, *49*(10–11), 1159–1173. [https://doi.org/10.1016/S0032-0633\(01\)00023-X](https://doi.org/10.1016/S0032-0633(01)00023-X)
- Paranicas, C., Mauk, B. H., Haggerty, D. K., Clark, G., Kollmann, P., Rymer, A. M., et al. (2018). Intervals of intense energetic electron beams over Jupiter's poles. *Journal of Geophysical Research: Space Physics*, *123*(3), 1989–1999. <https://doi.org/10.1002/2017JA025106>
- Parkinson, C. D., Stewart, A. I. F., Wong, A. S., Yung, Y. L., & Ajello, J. M. (2006). Enhanced transport in the polar mesosphere of Jupiter: Evidence from Cassini UVIS helium 584 Å airglow. *Journal of Geophysical Research: Planets*, *111*(E2). <https://doi.org/10.1029/2005je002539>
- Sinclair, J. A., Greathouse, T. K., Giles, R., Antuñaño, A., Fouchet, T., Bézard, B., et al. (2019). *IRTF-TEXES observations of stratospheric CH₃ and CH₄ emission at Jupiter's high latitudes*. AGU Fall Meeting Abstracts (Vol. 2019), pp. P21G–3444.
- Stallard, T. S., Miller, S., Cowley, S. W. H., & Bunce, E. J. (2003). Jupiter's polar ionospheric flows: Measured intensity and velocity variations poleward of the main auroral oval. *Geophysical Research Letters*, *30*(5), 1221. <https://doi.org/10.1029/2002GL016031>
- Swithenbank-Harris, B. G., Nichols, J. D., & Bunce, E. J. (2019). Jupiter's dark polar region as observed by the Hubble space telescope during the Juno approach phase. *Journal of Geophysical Research (Space Physics)*, *124*(11), 9094–9105. <https://doi.org/10.1029/2019JA027306>
- Szalay, J. R., Allegrini, F., Bagenal, F., Bolton, S. J., Bonfond, B., Clark, G., et al. (2020). Alfvénic acceleration sustains Ganymede's footprint tail aurora. *Geophysical Research Letters*, *47*(3), e86527. <https://doi.org/10.1029/2019GL086527>
- Tetrick, S. S., Gurnett, D. A., Kurth, W. S., Imai, M., Hospodarsky, G. B., Bolton, S. J., et al. (2017). Plasma waves in Jupiter's high-latitude regions: Observations from the Juno spacecraft. *Geophysical Research Letters*, *44*(10), 4447–4454. <https://doi.org/10.1002/2017GL073073>
- Vasyliunas, V. M. (1983). *Physics of the Jovian magnetosphere. 11 Plasma distribution and flow* (pp. 395–453). Cambridge University Press.
- Vogt, M. F., Bunce, E. J., Kivelson, M. G., Khurana, K. K., Walker, R. J., Radioti, A., et al. (2015). Magnetosphere-ionosphere mapping at Jupiter: Quantifying the effects of using different internal field models. *Journal of Geophysical Research: Space Physics*, *120*(4), 2584–2599. <https://doi.org/10.1002/2014JA020729>
- Vogt, M. F., Kivelson, M. G., Khurana, K. K., Walker, R. J., Bonfond, B., Grodent, D., & Radioti, A. (2011). Improved mapping of Jupiter's auroral features to magnetospheric sources. *Journal of Geophysical Research: Space Physics*, *116*(A3), A03220. <https://doi.org/10.1029/2010JA016148>

- Yung, Y. L., Gladstone, G. R., Chang, K. M., Ajello, J. M., & Srivastava, S. K. (1982). H₂ fluorescence spectrum from 1200 to 1700 Å by electron impact—Laboratory study and application to Jovian aurora. *The Astrophysical Journal Letters*, 254, L65–L69. <https://doi.org/10.1086/183757>
- Zhang, B., Delamere, P. A., Yao, Z., Bonfond, B., Lin, D., Sorathia, K. A., et al. (2020). *How Jupiter's unusual magnetospheric topology structures its aurora*. arXiv:2006.14834.